2018

Nanomaterial Charge-Dependent Platelet Activating Factor Receptor Agonism in Human Epidermal Cells

Shahryar Jamshed Qureshi
Wright State University

NANOMATERIAL CHARGE-DEPENDENT PLATELET ACTIVATING FACTOR RECEPTOR AGONISM IN HUMAN EPIDERMAL CELLS

A thesis submitted in partial fulfillment
of the requirements for the degree of
Master of Science

By

SHAHRYAR JAMSHED QURESHI

B.A, Miami University, 2015

2018

Wright State University

Wright State University

Graduate School

July 26, 2018

I HEREBY RECOMMEND THAT THE THESIS PREPAPERED UNDER MY SUPERVISION BY Shahryar Jamshed Qureshi ENTITLTED Nanomaterial Charge-Dependent Platelet Activating Factor Receptor Agonism in Human Epidermal Cells BE ACCEPTED IN PARTIAL FULFILLMENT OF THE REQUIREMENTS FOR THE DEGREE OF Master of Science

_____

Saber Hussain, Ph.D.
Thesis Director

_____

Jeffrey Travers, M.D. Ph.D.
Chair, Department of Pharmacology and Toxicology

Committee on
Final Examination

_____

Saber M. Hussain, Ph.D.

_____

Richard L. Salisbury, Ph.D.

_____

Mark Tyler Nelson, Ph.D.

_____

Terry L. Oroszi, Ed. D

_____

Jeffrey B. Travers, M.D. Ph.D.

_____

Barry Milligan, Ph.D.
Interim Dean, Graduate School

Abstract

Qureshi, Shahryar Jamshed. M.S. Department of Pharmacology and Toxicology, Wright State University, 2018. Nanomaterial Charge-Dependent Platelet Activating Factor Receptor Agonism in Human Epidermal Cells

Platelet Activating Factor (PAF) and its associated receptor, the PAF Receptor (PAFR), are important mediators of intercellular communication during an immune response. Once a physiological stimulus triggers an inflammatory response, epithelial, endothelial and immune cells synthesize and release PAF. PAF mediates the recruitment of immune cells, platelets, angiogenesis, expression of various genes, and increased PAF biosynthesis (Brown, 2006; Han, 2006; Whatley, 1988; Axelrod, 1988). In this study, we utilized HaCaT cells and a well characterized KB cell line derived from nasopharyngeal cells, which do not natively express the PAFR. KB cells had previously been transfected with a PAF receptor (KBP) or a mock transfection (KBM), yielding two cell lines. The KBM and KBP cell lines allow for a mechanistic *in vitro* assessment of charge-dependent nanoparticle (NP) mediated PAFR activation, where KBP cells should show more robust Interleukin-8 (IL-8) secretion than KBM cells. Furthermore, this cell model serves to identify PAFR agonist formation, which has been reported to be generated from cigarette smoke, ultraviolet B radiation, jet fuel, and other stimuli that result in oxidative stress. The PAFR is involved in clathrin-mediated endocytosis, yet the PAFR role in NP uptake has not been investigated. The ability of NPs to generate PAF agonists is not known and the mechanisms by which

they are internalized have yet to be fully understood. To investigate whether NP charge contributes to direct PAF-like lipid formation, KBM, KBP and HaCaT cell lines were exposed to 1 to 100µg/mL of 40nm Ag-NPs that were functionalized with either branched polyethyleneimine (BPEI) or citrate to give them a positive or negative surface charge, respectively. We demonstrated; a charge-dependent increase in NP-induced IL-8 production in KBP and HaCaT cells; indirectly measured an increased activation of the PAFR after 24 hours of exposure in KBP and HaCaT cells; dose-dependent uptake of NPs in all cell lines and increased reactive oxygen species (ROS) generation in KB cell lines only. Further analysis of NP-induced PAFR activation may grant us a better understanding of dermal inflammation and the potential role of PAF-like lipids in NP-mediated wound healing therapies.

Table of Contents

List of Figures

List of Tables

Introduction

Engineered Nanomaterials (ENM) and nanoparticles (NPs) are variously shaped and charged particles with on dimension that is less than 100 nanometers (nm). ENMs are intentionally formed materials (tubes, wires, spheres, etc.) that are applied towards the advancement of components and parts, known as nano-intermediates (coatings, textiles, electronics, etc.). These nano-intermediates are incorporated into nano-enabled products that surround us in our daily life and are utilized in many fields around the world today. NPs are naturally or incidentally formed materials (diesel exhaust, welding fumes, propellant exhaust, etc.) that sometimes are a result of ENM destruction (Ristovsky, 2006). The global nanotechnology market has been increasing seeing a rise with every passing year. The global nanocomposite market increased by $500 million USD between 2016 and 2017 (McWilliams, 2018), while the global nanomedical market increased by $17.5 billion USD from 2016 to 2017 (Evers, 2018).

The boom of nanotechnology and use of nano-enabled products in our society has driven the need to fully understand the potential toxicity of NPs. Nanotoxicology is the study of the potential toxicity of ENMs and NPs based on their physical and chemical properties. Investigating the implication of nano-scale particulate exposure is not only important for human health effects, but also for environmental health effects. Numerous studies have shown that ENMs and NPs toxic effects are dependent on their physical and

chemical characteristics (size, shape, chemistry, crystal structure, solubility, surface coating, surface charge, etc) (Posgai, 2011).

Nano-scale particulate exposure to the epithelium has been reported to cause oxidative stress and acute inflammation (Zhang, 2008; Samberg, 2010; Yazdi, 2010). Exposure to these particles can occur when one is in a combat environment, materials lab, industrial facilities, or at home. The respiratory and integumentary systems are the most probable routes of exposure, which is why it is important to understand the toxicological mechanisms that takes place during these exposures. Not only can we better prevent disease through understanding these mechanisms, we can also attempt to harness the ability of these particles to elicit desired physiological outcomes.

The precise mechanism of NP-induced inflammation in the human epithelium is not clear. To elucidate this mechanism, we investigate the involvement of the Platelet Activating Factor Receptor (PAFR), a G-Protein Coupled Receptor (GPCR), primarily expressed by endothelial, epithelial and immune cells (Whatley, 1989; McIntyre, 1987). The PAFR binds its natural ligand, Platelet Activating Factor (1-*O*-alkyl-2-acetyl-sn-glycerolphosphocholine; PAF) a phospholipid autacoid, which activates the PAFR and induces a potent paracrine cascade that mediates physiological and pathological conditions.

Upon activation, the PAFR elicits a cell-specific response dependent on the alpha subunit isoform of its heterotrimeric G-protein complex (Brown, 2006). PAFR's holding the pertussis toxin (Ptx)-sensitive $G\alpha_i$ subunit cause an inhibition of Adenylate Cyclase

(AC) activity, preventing conversion of Adenosine Triphosphate (ATP) to Cyclic Adenosine Monophosphate (cAMP). This inhibition also prevents the activation of the [cAMP]-dependent enzyme, Protein Kinase A (PKA), which primarily regulates carbohydrate and lipid metabolism (Brown, 2006; Ali, 1994; Ye, 1991). PAFR's holding the predominant, Ptx-insensitive, $G\alpha_q$ subunit activate Phospholipase C beta (PLCβ), located in the inner membrane, which hydrolyzes the inner membrane protein Phosphatidylinositol-4,5-bisphosphate (PIP2) into cytosolic Inositol-1,4,5-trisphosphate (IP3) and membrane bound Diacylglycerol (DAG). IP3 diffuses across the cytoplasm to bind to the Ins3P Receptor (Ins3PR), a glycoprotein receptor complex that acts as a ligand-gated Ca^{2+} channel, located on the Endoplasmic Reticulum (ER) (Hirafuji, 1988). This transient increase in intracellular Ca^{2+} propagates a myriad of cellular processes where Ca^{2+} acts as a second messenger (Barrett, 1984). In regards of the PAFR cascade, this Ca^{2+} activates a group of calcium-dependent cytosolic Phospholipase A_2 ($cPLA_2$), which translocates to the inner membrane to dock to PIP_2 or Ceramide-1-phospate for membrane binding and lipase activity (Six, 2003; Stahelin, 2007). Ca^{2+} also binds to Protein Kinase C (PKC), which diffuses to the inner plasma membrane to bind DAG, completing its activation (Kim, 2013). The PAFR downstream biological effects include platelet aggregation, neutrophil chemotaxis, chemokine secretion, PAF biosynthesis, growth signaling, cytoskeletal rearrangement, Reactive Oxygen Species (ROS) generation, leukocyte activation and acute inflammation (Brown, 2006; Han, 2006; Whatley, 1988; Axelrod, 1988).

Due to PAF's potent physiological activity at picomolar concentrations, the understanding of regulated and unregulated PAF biosynthesis is important. The most common natural isoforms of PAF have been identified as C_{16}-PAF and C_{18}-PAF, however C_{16}-PAF is the predominant molecular species in human epithelial and endothelial cells (Holtzman, 1991). The glycerol backbone of PAF holds a 16:0 or 18:0 fatty acid at its *sn-1* position, a phosphatidylcholine moiety at its *sn-3* position and an acetyl group, integral for its function, at the *sn-2* position (Marathe, 1999; Shen, 1987). Unlike most lipid mediators, PAF uniquely undergoes a highly conserved ether linkage rather than an ester linkage at its *sn* positions. The two-known regulated biosynthetic pathways responsible for the generation of C_{16}-PAF and C_{18}-PAF are the remodeling pathway and the *de novo* pathway. The remodeling pathway, which is the primary PAF biosynthetic pathway, involves the removal of an unsaturated fatty acid (commonly 20:4) from the *sn-2* position of an ether glycerophosphocholine (GPC) by PLA_2, yielding arachidonic acid and an ether lyso-GPC (lyso-PAF). Lyso-PAF is acetylated by at the *sn-2* position by Lyso-PAF Acetyltransferase (LPCAT) and forms PAF. The *de novo* pathway utilizes a two to three step enzymatic process that converts a 16:0 or 18:0 lyso-phospholipid into a 1-alkyl-2-acetyl glycerol, which is used to generate PAF through the action of a phosphocholine transferase enzyme (Flamand, 2009; Blank, 1987; Ramesha, 1986; Chilton, 1984). C_{16}-PAF and C_{18}-PAF are considered exclusive ligands to the PAFR and are regulated by the enzyme PAF-Acetyl Hydrolase (PAF-AH). Outside of these regulated synthesis pathways, there is ongoing investigation into the generation and effects of PAF-like lipids, capable of

acting as PAFR agonists. These PAF-like lipids have been identified as oxidized-GPCs (OxGPC) which hold variation in length and saturation of their fatty acid tails, yet conserve the acetyl and phosphatidylcholine groups at the *sn-2* and *sn-3* positions, respectively. Factors such as Ultraviolet-B (UVB) radiation, cigarette smoke and lipoteichoic acid have been reported as a few generators of OxGPCs through unregulated lipoxygenase-mediated or free radical-mediated processes (Da Silva, 2017; Sahu, 2013; Yao, 2009; Travers, 1999).

A well-documented cellular response to silver (Ag) NP exposure is oxidative stress (Shvedova, 2011; Foldbjerg, 2009; Carlson, 2007). The potential of charged Ag-NPs to either directly oxidize GPCs, indirectly form OxGPCs through free radical generation or activate the PAFR through interactions with the NP's protein corona have not been investigated. Ag NPs were used because of their increasing incorporation into biomedical, consumer and wound healing products, as well as their well-known antibacterial properties (Dunn, 2004; Khundkar, 2009). In this study, we utilized two well characterized nasopharyngeal cell lines (KB) that either received a stable transfection of the PAFR (KBP) or a mock transfection (KBM). We also utilized the immortalized human keratinocyte HaCaT cells line which endogenously expresses the PAFR. We investigated the potential of positively and negatively charged Ag-NPs to form PAF-like lipids in KBM, KBP and HaCaT cells. The aims of this study were to understand: the role of Ag-NP charge in PAFR activation and PAF-like lipid formation in KBM, KBP and HaCaT cells; the role of ROS in the inflammation response to charged Ag-NPs exposure in KBM, KBP and HaCaT cells;

and the endocytic potential of PAFR-positive and negative cells during charged Ag-NP exposure.

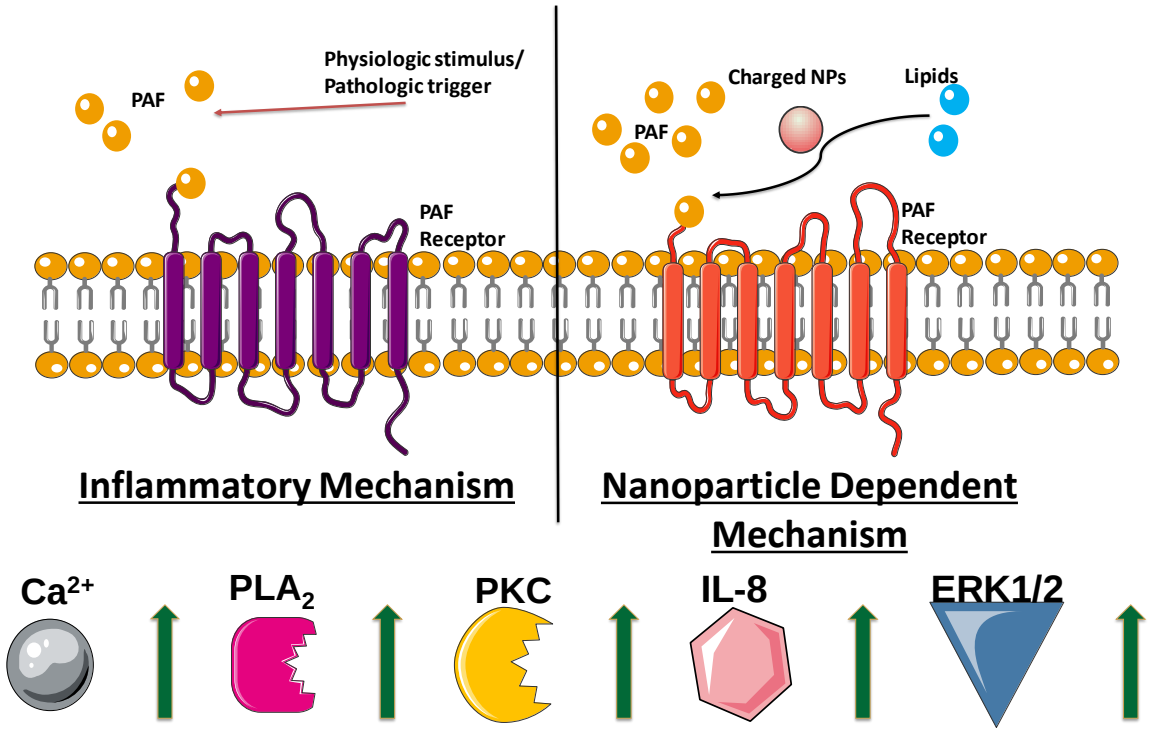

Figure 1. Hypothesized mechanism of NP-dependent formation of PAF-like lipids.

Methods and Materials

Materials and Reagents

40nm Ag-Branched Polyethyleneimine (BPEI) and 40nm Ag-Citrate nanoparticles were obtained from NanoComposix (San Diego, CA). N-Acetyl-Cysteine (NAC) and tetradecanoyl phorbol acetate (TPA) was obtained from Sigma-Aldrich (Saint Louis, MO). DMEM High Glucose media, heat inactivated Fetal Bovine Serum (HI-FBS), penicillin/streptomycin (P/S), Hanks Balanced Salt Solution (HBSS), Bovine Serum Albumin (BSA) and 0.25% Trypsin-EDTA were all acquired from Gibco inc. (ThermoFisher Scientific, USA). The PAFR agonist used in these studies was Carbamoyl-PAF (CPAF; 1-hexadecyl-2-*N*-methylcarbamoyl glycerophosphocholine) which was purchased from Cayman Chemical (MI, USA).

Dynamic Light Scattering (DLS)

Nanoparticles hydrodynamic diameter and surface charge (zeta potential) were determined by analyzing a 100ug/mL solution of NPs suspended in H_2O, HBSS or supplemented media in disposable cuvettes with a Zetasizer Nano ZS (Malvern Instruments, Malvern, UK).

Cell Culture

KBM and KBP cells were kindly provided by Dr. Jeffrey Travers (Pharmacology and Toxicology Department, Boonshoft School of Medicine, Wright State University, OH, USA) and HaCaT cells were purchased from ATCC (Manassas, VA). KBM, KBP and

HaCaT cell lines were cultured in DMEM high glucose medium in individual T-75 flasks and incubated at 37°C in a 5% CO_2 atmosphere. DMEM media was supplemented with 10% HI-FBS, 1% P/S and 1% L-Glutamine. KBM, KBP and HaCaT cells were seeded individually into 48-well plates at 40,000cells/cm^2. Cells were trypsinized with 0.25% EDTA-free Trypsin once at 80% confluency and a cell count was determined using a Cellometer Vision (Nexcelom Bioscience, Lawrence, MA). Once seeded, cells were incubated for 24 hours for maximum adherence before experimental exposure.

Upon 24-hour exposure to nanoparticles, supernatant was collected and stored at 4°C for IL-8 quantification. Cells in each well were washed twice with 1xPBS (200µL), trypsinized (100µL) and neutralized with HI-FBS containing media (200µL) for flow cytometry. The remaining cells were stored at 4°C in 15mL conical tubes for uptake analysis.

Flow Cytometry

A Guava 12-HT Easycyte Flow cytometer (EMD Millipore-Sigma, USA) was used to determine cell count. 48-well plates were spun down at 600 rcf (relative centripetal force) using a plate centrifuge to pellet the non-adherent (dead) cell fraction. The exposure media was then aspirated and rinsed twice with 1xPBS, with a plate centrifuge step before each aspiration. Cells were then trypsinized and subsequently neutralized after 5 minutes at 37°C in a 5% CO_2 atmosphere. 60µL of the live and dead cell fractions of each well were placed in a U-bottom 96-well plate (EMD Millipore-Sigma, USA) and was followed with

60µL of Guava Viacount solution (EMD Millipore-Sigma, USA) and incubated at 37°C in a 5% CO_2 atmosphere for 5 minutes. The Guava flow cytometer was flushed, primed and gated prior to running the plate. Following incubation, the 96-well plate was loaded into the cytometer with the blue laser with PM1 voltage of 450, PM2 voltage set to 550.

Inductively Coupled Plasma – Mass Spectrometry (ICP-MS) Sample Preparation

A NexION 300D (Perkin Elmer) was utilized to quantify the uptake of nanoparticles. The remaining volume of live and dead cell fractions in the 48-well plates that were not used for flow cytometry were placed into individual 15mL conical tubes and prepared for ICP-MS analysis. Organic content was dissolved in concentrated HCl (37%), HNO3 (60%) and diluted Triton-X 100 (1%), reagents were added at 8.1%, 1.4%, and 5.0% of the total 10mL ICP-MS sample volume. Bismuth was used as an internal standard and added at 2% of ICP-MS sample volume. Samples were incubated for 30 minutes to ensure all organic material was dissolved before running through a NexION 300D.

IL-8 Analysis

IL-8 secretion was quantified via an enzyme linked immunosorbent assay (ELISA; Human IL-8 ELISA MAX Deluxe Kit, Biolegend Inc., USA) according to the provided instructions. ELISA plates were read using a Flexstation 3 Plate Reader (Molecular Devices LLC, San Jose, USA) at an absorbance of 450nm and the obtained values were standardized by normalizing to total cell count.

Reactive Oxygen Species (ROS) Analysis

ROS was analyzed using a 5mM dichlorofluorescin diacetate (H_2DCF-DA) probe incubated for 30 minutes in 96-well cell culture plates prior to NP exposure. After exposure, fluorescence was read using a Flexstation 3 Plate Reader measured at a wavelength of 480nm at 0, 2, 4, 6, 8 and 24 hours. H_2O_2 was used as a positive control in each experiment to control for probe reactivity and NAC was used as a negative control in each experiment to control for ROS-mediated probe reactivity.

PAF-R Immunostaining and Confocal Imaging

KBM and KBP cells were imaged for PAFR protein expression through fluorescence microscopy using an Olympus IX81 Confocal Laser Scanning Microscope (Olympus Inc., USA). Cells were stained for the PAFR using an Anti-PAF Receptor antibody (ab104162; Abcam plc., USA), actin was stained or using Alexafluor phalloidin 488 actin stain (1:100 dilution; Invitrogen, USA) and DNA was stained using DAPI stain (1:1500 dilution). KBM and KBP cells were seeded on a round glass substrate placed within a 12-well plate. Cells were first fixed in paraformaldehyde (4%) for 5 minutes, followed by washing with PBS. Cell membranes were then permeabilized using Triton-X 100 (0.1%) for 15 minutes at 37 degrees Celsius, subsequently washed with PBS, and blocked using BSA (1%) for 30 minutes. Cells were then incubated in Anti-PAFR antibody (1:1000) overnight. After overnight incubation the antibody was aspirated and washed three times with 1x PBS for five minutes each. The secondary antibody, Alexa Fluor 568 (ab175471; 1:1000; Abcam plc., USA) was incubated for one hour at room temperature

and subsequently washed three times with 1xPBS for 5 minutes each. After secondary antibody incubation, DAPI and Alexafluor 488 phalloidin stain was applied for 30 minutes. After staining, cells were washed three times with 1xPBS, coated with a drop of Prolong Gold mounting media (Invitrogen, USA), and secured to a glass coverslip. The next day, excess mounting media was removed, and the edges of the sample were sealed with clear finger nail polish. Images were then taken using a UPLFLN 40x Oil objective with a numerical aperture of 1.3. The laser settings are as follows: 405nm set at 15% and 450 volts; 488nm set at 25% and 510 volts; 543nm set at 30% and 685 volts.

Transmission Electron Microscopy (TEM)

Cell samples were fixed in 2% paraformaldehyde (Electron Microscopy Supplies, USA) and 2.5% glutaraldehyde (Electron Microscopy Supplies, USA) for 15 min. at room temperature, and subsequently stained with 1% osmium tetroxide (Electron Microscopy Supplies, USA) for 1 hour. Serial dehydrations were performed with 30%, 70%, 95%, and 100% ethanol. Following dehydration, samples were placed in a 1:1 ratio of 100% ethanol and LR White resin for 1 hour at room temperature, then into 100% LR White resin (Electron Microscopy Supplies, USA) and cured overnight at 60°C and -25psi. Cured blocks were sectioned using a Leica Ultramicrotome UC7 (Leica Inc., USA), and 70nm sections were deposited onto copper grids with carbon film. Imaging and elemental analysis was performed on the Zeiss Gemini STEM (Zeiss, USA).

Results

Characterization of 40nm Ag-BPEI and 40nm Ag-Citrate NPs and KB Cell Lines

The hydrodynamic diameter, surface charge (ζ-potential) and polydispersity index (PDI) of Ag-NPs are displayed in Table 1. The desired ζ-potential of NPs in solution was only attained when using HBSS as the vehicle, with Ag-BPEI NPs holding a positive charge of 22.2 ± 0.417mV and Ag-Citrate NPs holding a negative charge of -30.5 ± 3.16mV. TEM images of 40nm Ag-BPEI and 40nm Ag-Citrate NP, as engineered, are shown in Figure 2, with their respective surface functionality's chemical structure.

		D_H (Mean ± SEM)	**ζ-Potential** (Mean ± SEM)	**PDI** (Mean ± SEM nm)
Water	*40nm Ag-BPEI*	45.81 ± 0.877	34.7 ± 0.611	0.159 ± 0.002
	40nm Ag-Citrate	43.33 ± 0.744	-37.8 ± 0.371	0.132 ± 0.001
Media	*40nm Ag-BPEI*	201 ± 0.881	-8 ± 1.40	0.191 ± 0.008
	40nm Ag-Citrate	112.5 ± 1.1	-11 ± 0.12	0.27 ± 0.003
HBSS	*40nm Ag-BPEI*	88.36 ± 1.47	22.2 ± 0.417	0.252 ± 0.003
	40nm Ag-Citrate	287.3 ± 13.8	-30.5 ± 3.16	0.253 ± 0.01

Table 1. The hydrodynamic diameter (D_H), surface charge (ζ -potential; mV) and polydispersity index (PDI) of 40nm Ag-BPEI and 40nm Ag-Citrate in water, DMEM media and HBSS.

KBM and KBP cell lines were stained for the PAFR, actin and nucleus at normal conditions to confirm the stable expression of the PAFR. In Figure 3, confocal images

show membrane localization and qualitative confirmation of the expression of the PAFR in, PAFR-positive, KBP cells but not in, PAFR-negative, KBM cells. We also observed no difference between morphology of the two cell lines

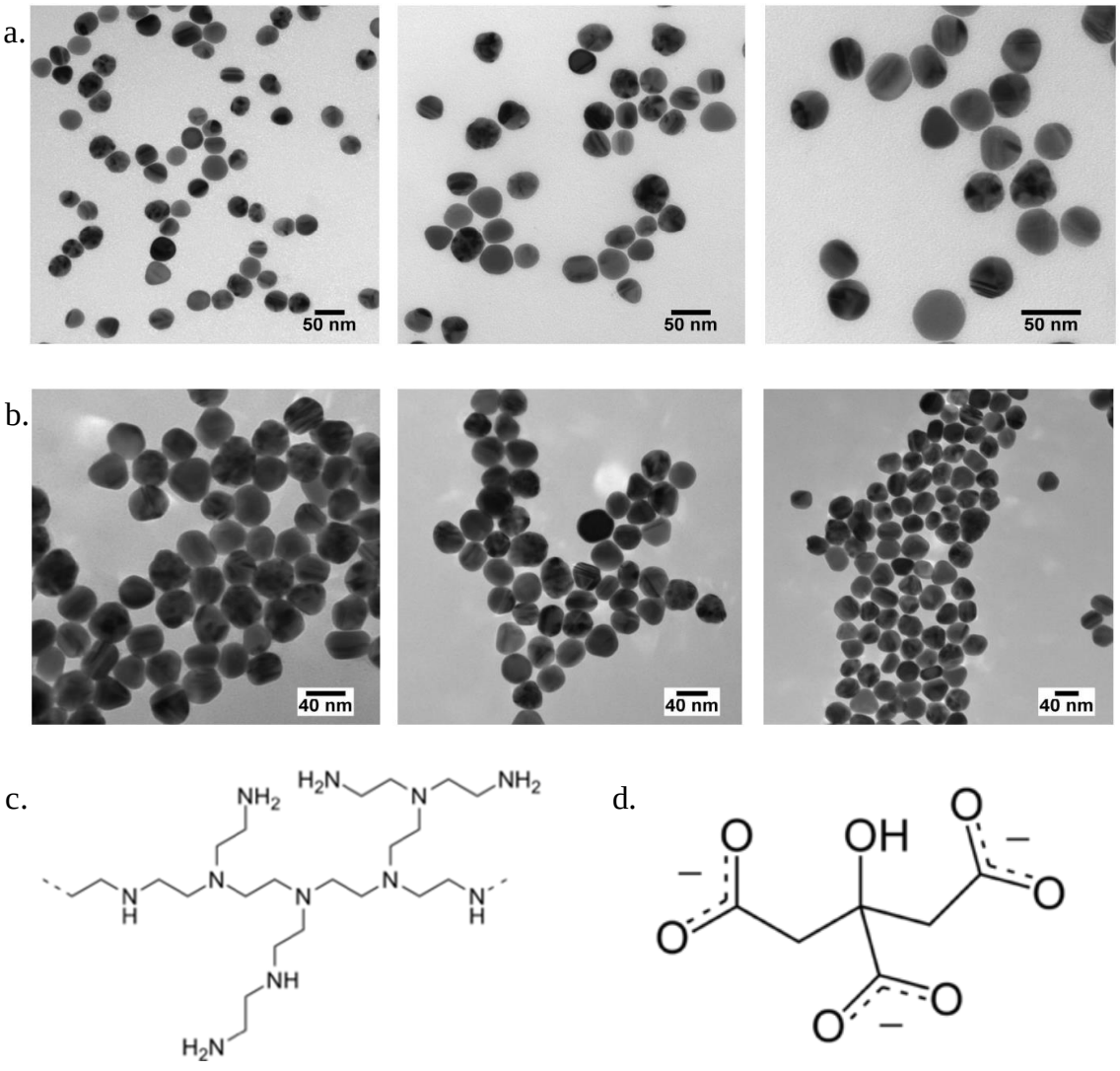

Figure 2. TEM images of 40nm Ag-BPEI (a) and 40nm Ag-Citrate NPs as engineered. The surface functionalization and chemical structure of branched polyethyleneimine (c) and citrate (d) are also provided. (Images taken from Nanocomposix)

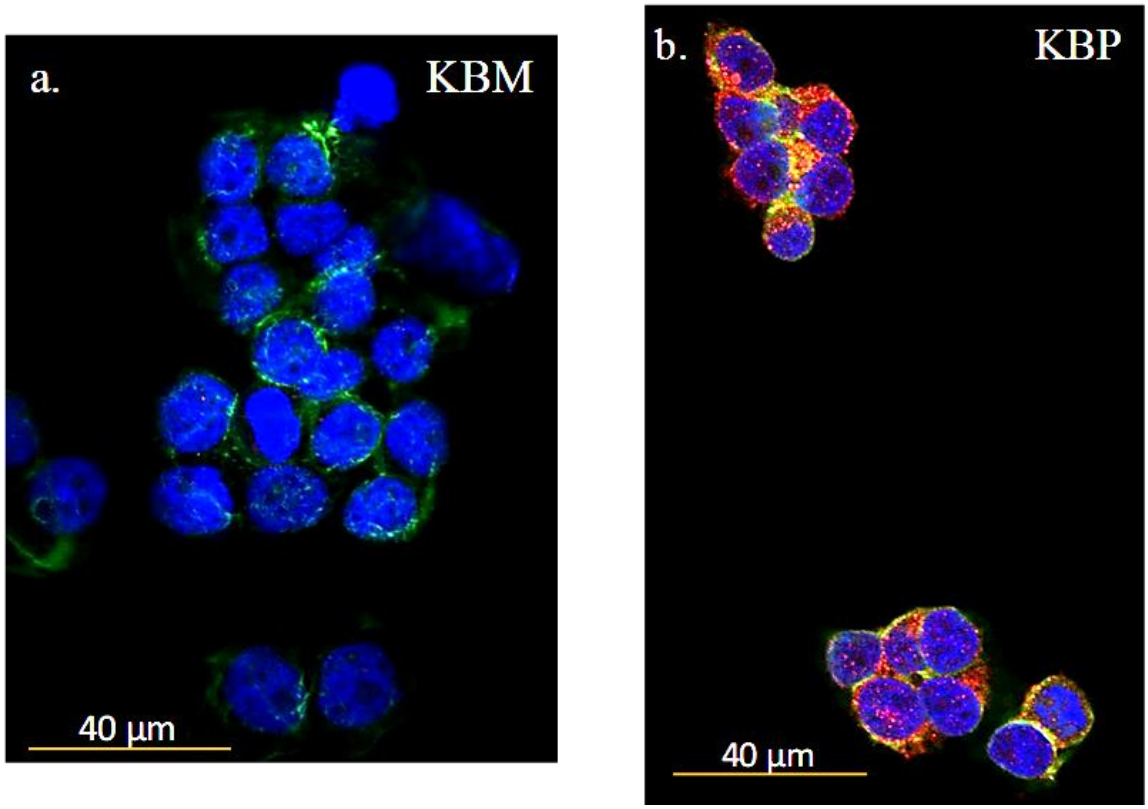

Figure 3. Confocal images of KBM and KBP cells stained for the PAFR (red), actin (green) and nucleus (blue).

Dose-Dependent IL-8 Secretion in PAFR Transfected Cells 24 Hours Post-Exposure to Charged Ag-NPs

IL-8 secretion was used as a direct indicator of inflammation as well as an indirect indicator of PAFR activation. PAFR-negative KBM cells showed no significant increase in IL-8 secretion in response to positively or negatively charged Ag-NPs at 1, 2.5, 5, 10 and 100µg/mL (Figure 4a). We observed a significant dose-dependent increase in IL-8 secretion in PAFR-positive KBP cells 24 hours post-exposure to 5 and 10µg/mL concentrations of positively charged Ag-BPEI NPs, yet this effect was not seen in response

to negatively charged Ag-Citrate NPs (Figure 4b). As expected, KBM and KBP cells showed significant secretions of IL-8 in response to 100nM of TPA, however only KBP cells responded to 100nM of the PAFR agonist, CPAF. Interestingly, we observed that concurrent 10µg/mL Ag-NP treatment with CPAF led to a suppression of IL-8 secretion and PAFR activation. Concurrent Ag-BPEI/CPAF exposure brought IL-8 secretion levels

to non-significant levels (Figure 4b), whereas concurrent Ag-Citrate/CPAF exposure significantly suppressed IL-8 secretions when compared to CPAF exposure.

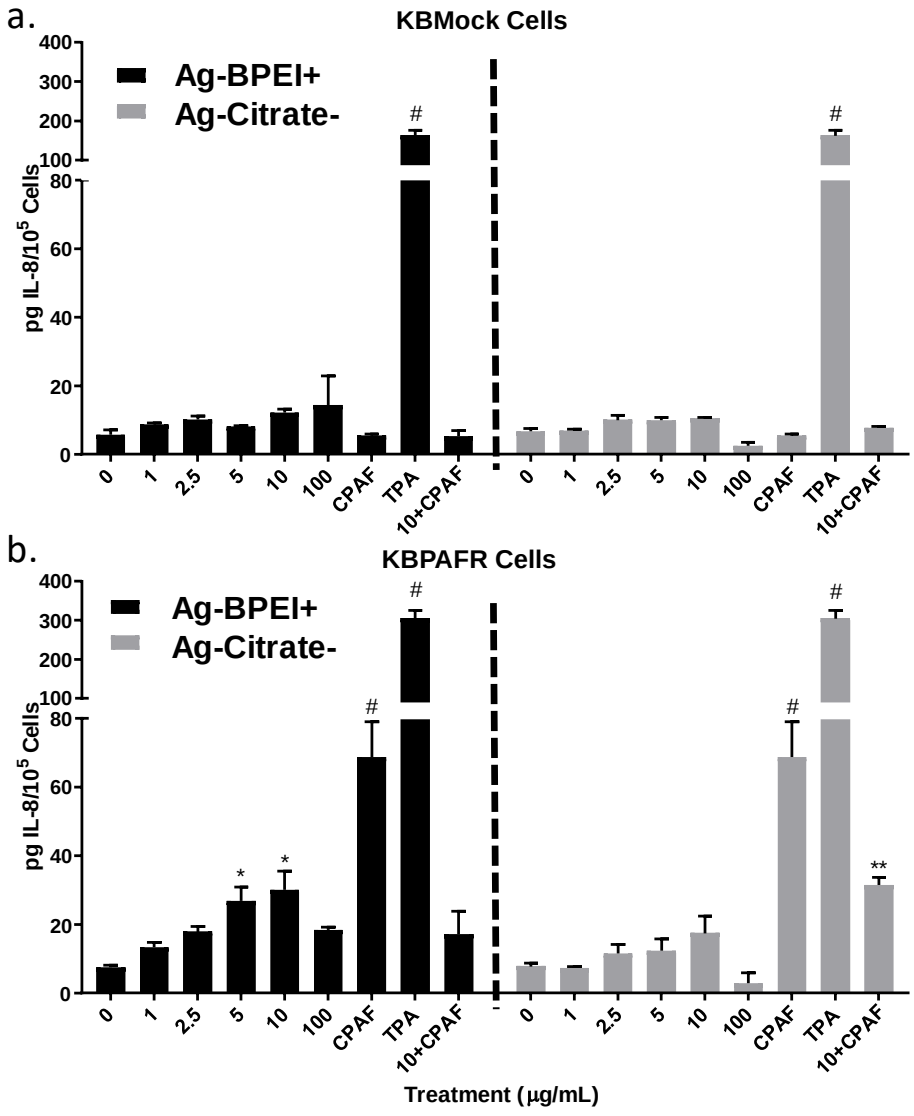

*Figure 4. IL-8 secretion 24 hours post-exopsure to 40nm Ag-BPEI and 40nm Ag-Citrate NPs in KBM (a) and KBP (b) cells. All treatments were compared to the 0 control within groups using a one-way ANOVA (Dunnets test; mean ± SEM, n=3 experiments; p<0.05 = *; p<0.01 = **; p<0.0001 = #)*

PAFR-Dependent IL-8 Secretion During Positively Charged Ag-NP Exposure

We compared the IL-8 secretion 24 hours post-exposure and found that the KBP cells secreted significantly higher levels of IL-8 than KBM cells during exposure to Ag-BPEI NPs but not to Ag-Citrate NPs (Figure 5a). Ag-BPEI NPs elicited significantly higher IL-8 secretion in KBP cells at 5 and 10µg/mL dosages whereas Ag-Citrate NPs elicited significantly higher IL-8 secretions in KBP cells during 10µg/mL/CPAF exposure in KBP cells (Figure 5b). In Figure 5a, we see a full suppressive effect of IL-8 secretion during

concurrent exposure of 10µg/mL Ag-BPEI and CPAF. This effect also exists in during concurrent Ag-Citrate and CPAF exposure, but to a lesser extent (Figure 5).

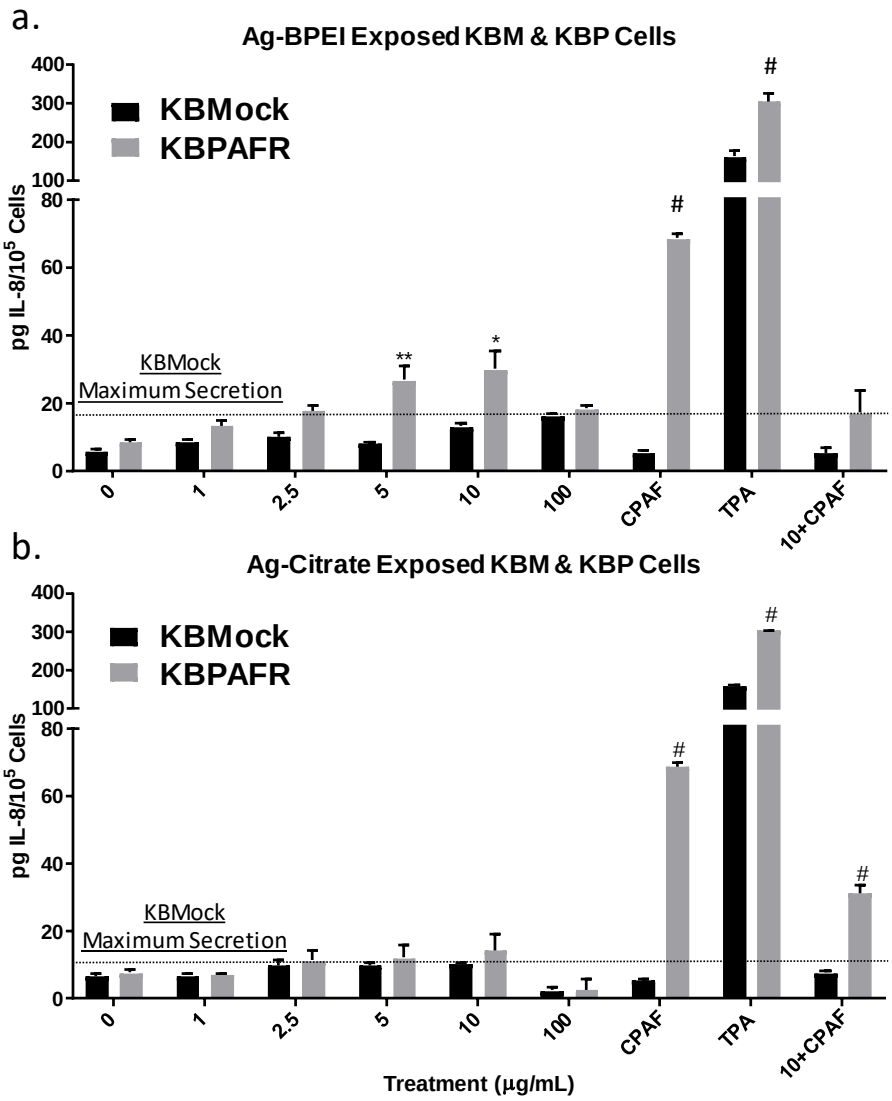

*Figure 5. IL-8 secretion 24 hours post-exopsure to 40nm Ag-BPEI (a) and 40nm Ag-Citrate (b) NPs in KBM and KBP cells. All treatments were compared between groups using a two-way ANOVA (Bonferroni test; mean ± SEM, n=3 experiments; p<0.05 = *; p<0.01 = **; p<0.0001 = #)*

PAFR-Dependent ROS Generation During Charged Ag-NP Exposure in Nasopharyngeal Cells

To investigate the magnified NP-induced inflammation in KBP cells, we analyzed ROS generation from 0 to 24 hours post-exposure to a 10μg/mL dose of NPs in KBM and KBP cells. In KBM cells, significant ROS generation was only seen at 2 hours post-exposure to Ag-BPEI NPs and at 8 and 24 hours post-exposure to Ag-Citrate NPs (Figure 6). In KBP cells, we found sustained ROS generation when exposed to Ag-BPEI from 2 to 24 hours post-exposure and significant ROS generation to Ag-Citrate NPs beginning from 4 to 24 hours post-exposure (Figure 6). We witnessed a sharp increase of ROS generation in response to Ag-Citrate NPs starting at 8 hours post-exposure in KBM cells and at 6 hours post-exposure in KBP cells. Both KBM and KBP cells exposed to Ag-BPEI saw a transient

elevation of ROS followed by a quick drop off seen at 2 hours in KBM cells and 4 hours in KBP cells (Figure 6).

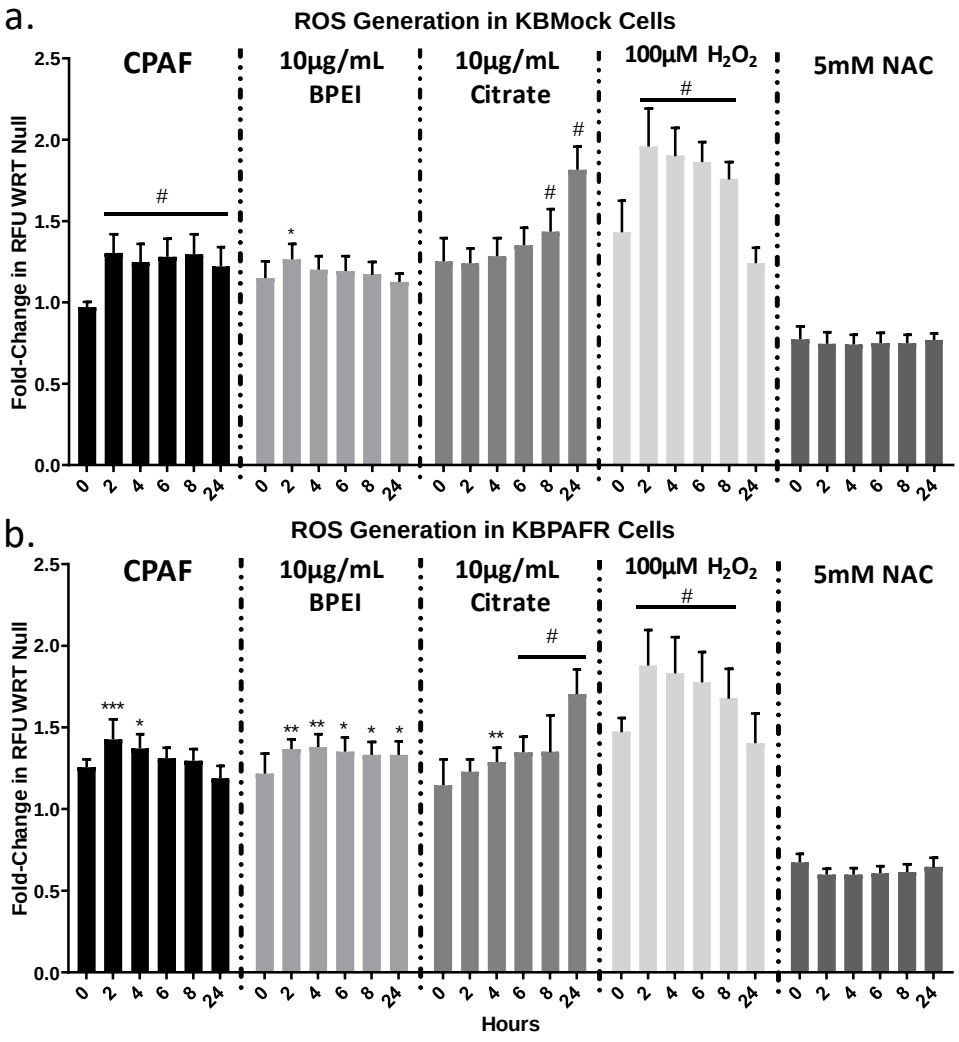

*Figure 6. ROS generation in KBM (a) and KBP (b) cells exposed to 100nM CPAF, 10µg/mL Ag-BPEI, 10µg/mL Ag-Citrate, 100uM H_2O_2 or 5mM NAC solution. Data is represented as fold change from the untreated control from each hour. All treatments were compared to the 0-hour reading within treatment groups using a one-way ANOVA (Dunnets test; mean ± SEM, n=3 experiments; p<0.05 = *; p<0.01 = **; p<0.0001 = #)*

Cell Line Dependence of IL-8 and ROS generation

To confirm PAFR involvement during charged Ag-NP exposure, we utilized human keratinocyte HaCaT cells, which endogenously expresses the PAFR. As expected, we found significant IL-8 secretion during 100nM CPAF exposure. Significant IL-8 secretion was only seen at the 10µg/mL Ag-BPEI exposure, however no significant IL-8 secretion was seen at any concentration during Ag-Citrate exposure (Figure 7). There was a significant and familiar suppression of IL-8 during concurrent 100nM CPAF and 10µg/mL Ag-BPEI and Ag-Citrate treatments (Figure 7). HaCaT cells showed significant ROS generation to CPAF exposure at 2 hours and to 10µg/mL Ag-Citrate at 24 hours, yet showed no significant ROS generation to 10µg/mL Ag-BPEI exposure (Figure 8).

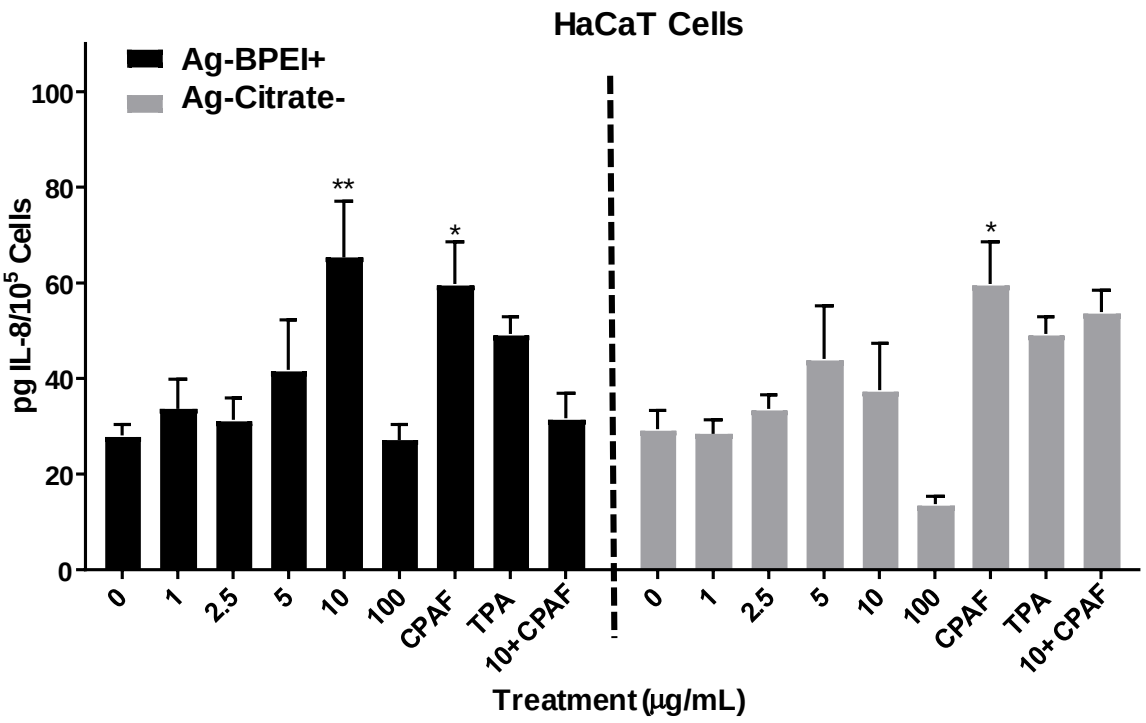

*Figure 7. IL-8 secretion 24 hours post-exopsure to 40nm Ag-BPEI and 40nm Ag-Citrate NPs in HaCaT cells. All treatments were compared to the 0 control within NP groups using a one-way ANOVA (Dunnets test; mean ± SEM, n=3 experiments; $p<0.05$ = *; $p<0.01$ = **)*

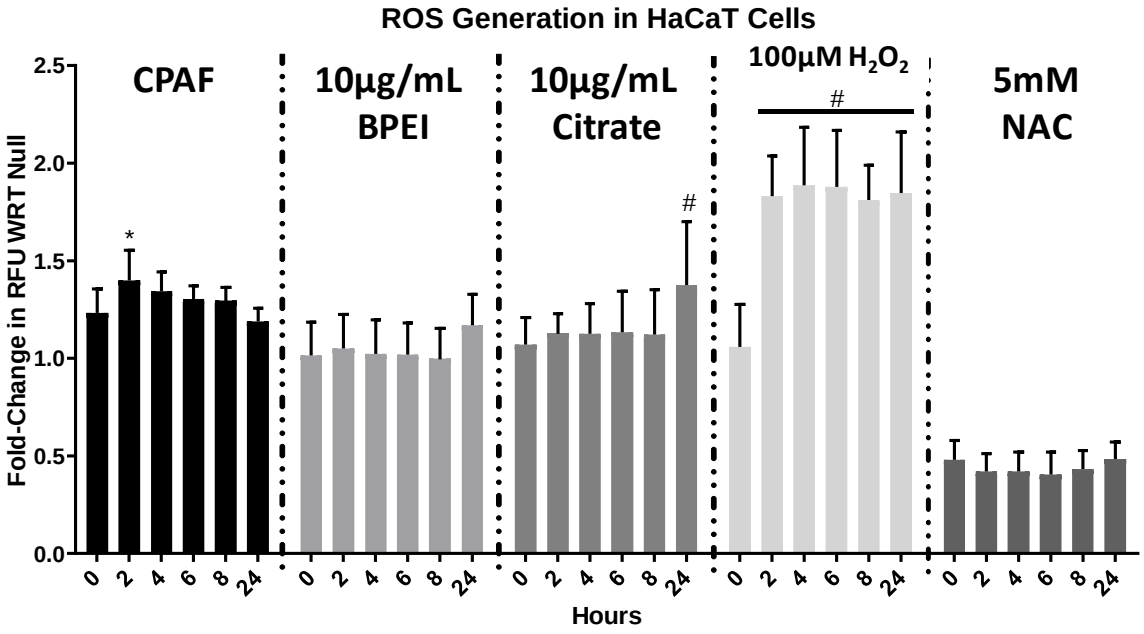

*Figure 8. ROS generation in HaCaT cells exposed to 100nM CPAF, 10µg/mL Ag-BPEI, 10µg/mL Ag-Citrate, 100uM H_2O_2 or 5mM NAC solution. Data is represented as fold change from the untreated control from each hour. All treatments were compared to the 0 hour reading within treatment groups using a one-way ANOVA (Dunnets test; mean ± SEM, n=3 experiments; $p<0.05$ = *; $p<0.0001$ = #)*

PAFR-Independent Uptake of Charged Ag-NPs at 24 Hours Post-Exposure

To further investigate the role of the PAFR in charged NP-induced inflammation, we measured charged Ag-NP uptake in KBM, KBP and HaCaT cell lines. ICP-MS results indicated a PAFR-independent endocytic potential of KBM, KBP and HaCaT cells 24 hours post-exposure. A dose-dependent internalization of Ag ions was detected in all cell types at all dosages, with significant internalization at the 100µg/mL dosages. No significant difference of Ag-NP internalization was detected between cell types (comparison not shown). To confirm the PAFR-independent uptake of Ag-NPs, KBM cells were exposed to 10µg/mL Ag-BPEI, fixed and prepared for TEM imaging. In Figure 10, we see internalized Ag-NPs contained in vesicles within KBM cells 8 hours post-exposure.

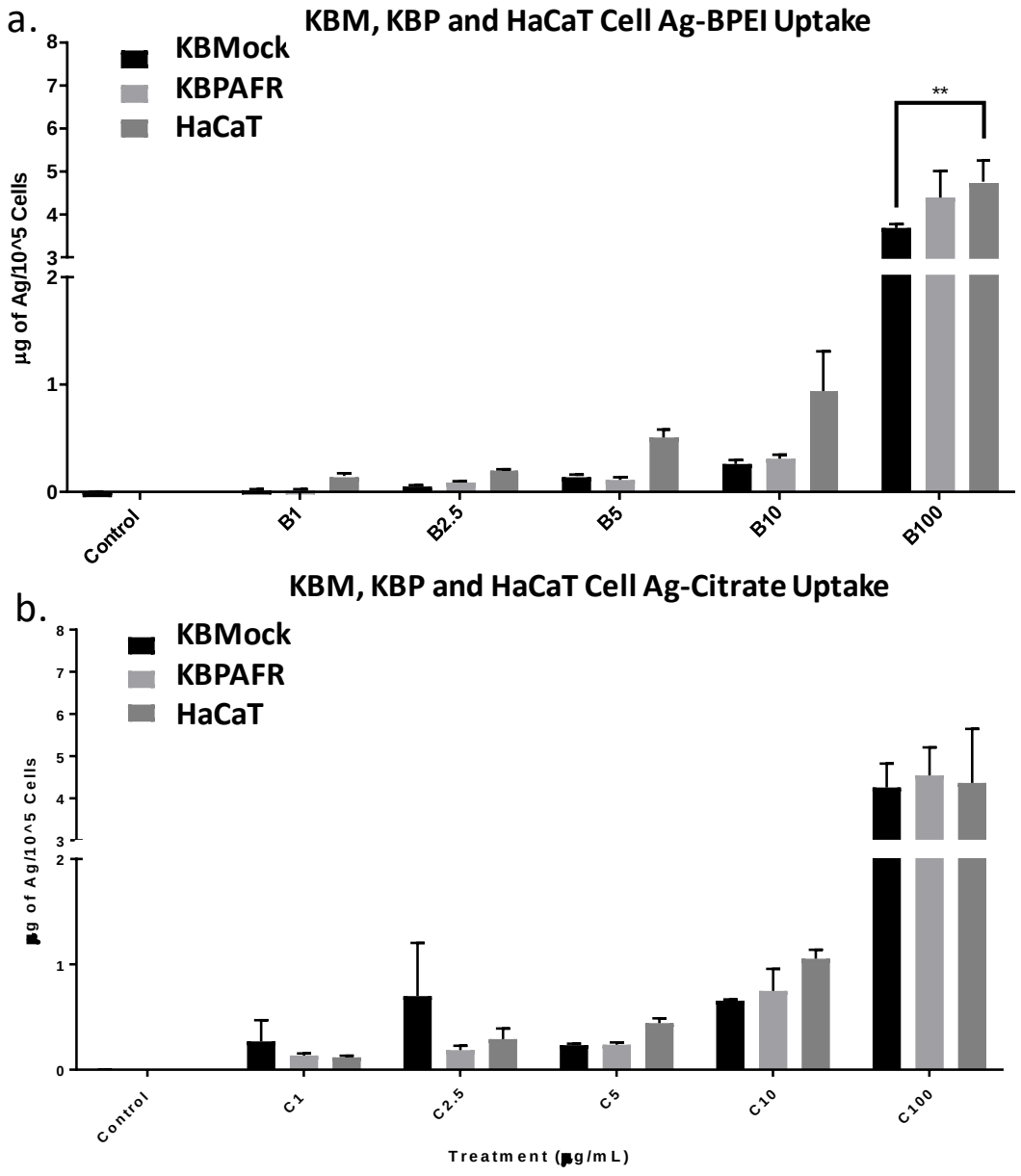

*Figure 9. ICP-MS data showing internalized concentration of Ag ions per 100,000 cells for KBM (a), KBP (a) and HaCaT (b) cells. All treatments were compared to the 0 control within groups using a two-way ANOVA (Bonferonni test; mean ± SEM, n=3 experiments; $p<0.01$ = **)*

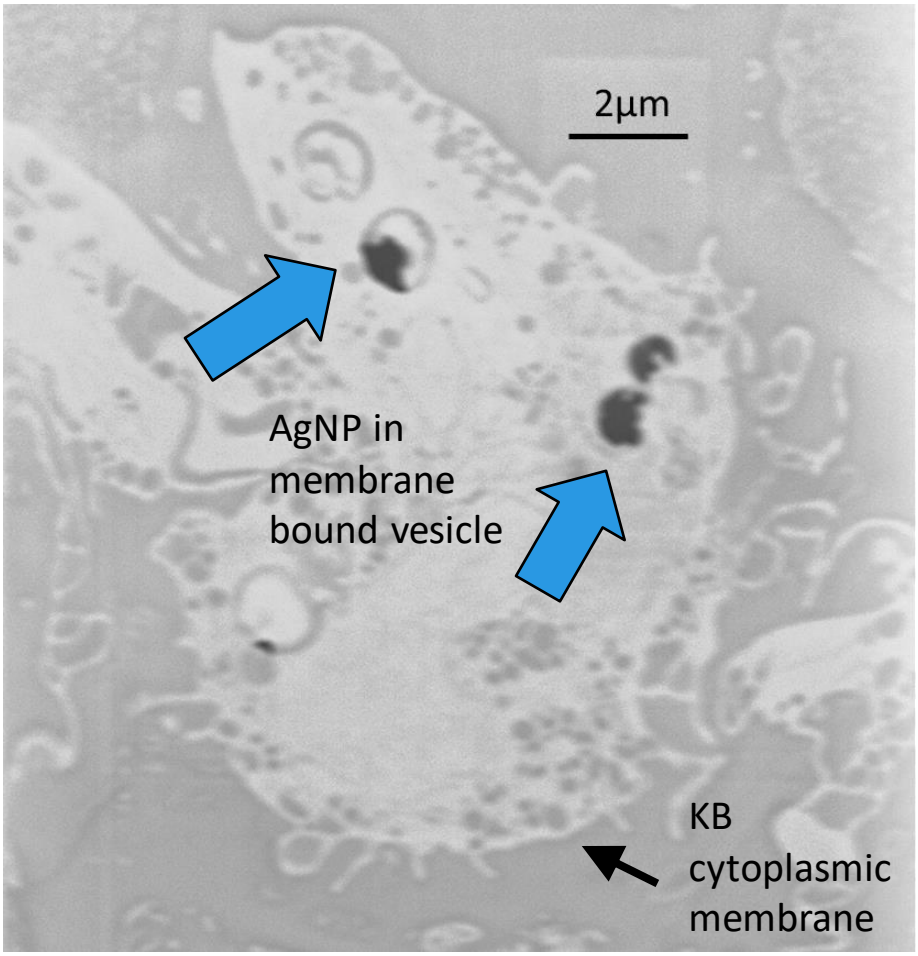

Figure 10. TEM image of KBM cell exposed to 10µg/mL Ag-BPEI NPs for 8 hours.

Discussion

The role of the PAFR in NP-mediated inflammation has not been investigated in the past, yet it has been extensively reported that exposure of charged and neutral nano-scale particulate to human keratinocytes leads to oxidative stress and inflammation (Samberg, 2010; Schaeublin, 2010; Miura, 2009). We wanted to investigate whether charged NPs are directly (Ag ion-mediated/protein corona-mediated lipid peroxidation) or indirectly (ROS-mediated lipid peroxidation) involved in the phenomenon of PAF-like lipid formation. To study this agonist formation, we utilized a unique model system to study PAFR activation. This system utilized KB, human nasopharyngeal, cells that do not express the PAFR in their native form. A group of KB cells were transduced with PAFR cDNA and the other group was transduced with control cDNA to yield PAFR-positive KBP cells and PAFR-negative KBM cells (Figure 3). The KB-PAFR model system is an excellent model to use when studying PAF-like lipid formation because of the model's use of a downstream effect of PAFR activation in epithelial cells, IL-8 secretion, which promotes the recruitment of neutrophils to the site of inflammation (Jeon, 2002). Thus, we measured and utilized IL-8 concentrations from the supernatant of exposed cell cultures as a surrogate of PAFR agonist activity (Figure 11). Another downstream effect of PAFR activation is the production of ROS, which we also utilized as an indirect measure of PAFR activation.

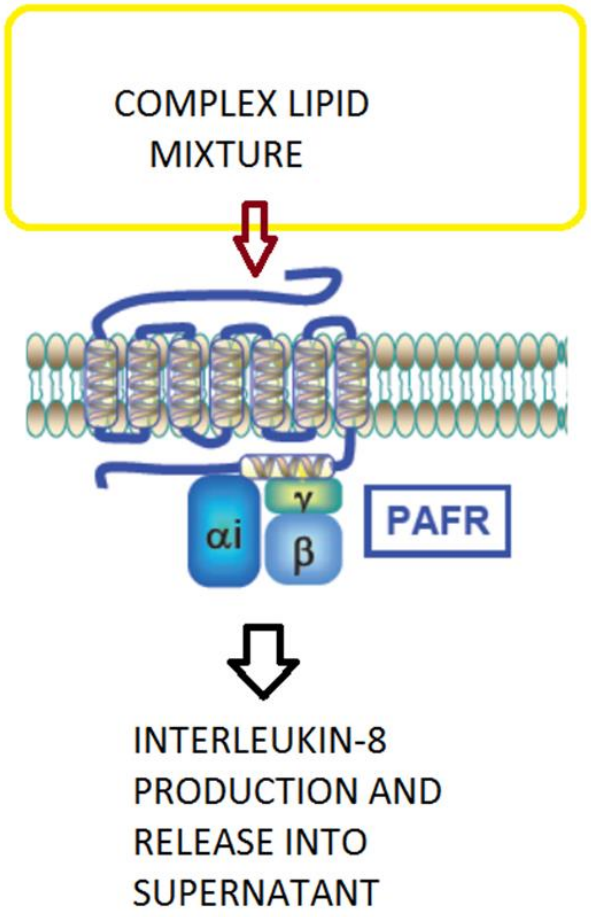

Figure 11. The KB-PAFR model system. (Image courtesy of Dr. Jeffrey Travers)

During characterization of the Ag-BPEI and Ag-Citrate NPs, we aimed to keep the NPs respective surface charge intact. When in DMEM high glucose medium supplemented with 1, 5 or 10% FBS, Ag-BPEI NPs lost their positive surface charge, presumably due to proteins from the FBS coating the NPs (Data not shown). To amend this, we utilized HBSS as the exposure medium, which allowed both NPs to maintain their respective surface charge (Table 1). HBSS is a Ca^{2+}/Mg^{2+}-containing isotonic salt solution which provides no

nutrition for cells and may have skewed cell viability after 24 hours. Since we were not interested in charged NP cytotoxicity, we focused on the ability of charged NPs to illicit the formation of PAF-like lipids. Using Ag NPs in this study did pose challenges due to their toxic potential making it difficult when discerning the effect of charge in PAFR activation.

Due to the potency of PAF, low levels of unregulated PAF-like lipid formation can lead to toxicity in the form of chronic inflammation. In this mechanistic study, we show support for positively charged 40nm Ag-BPEI NPs directly causing PAF-like lipid formation from the significant increase of IL-8 secretion seen at a 10µg/mL dose 24 hours post-exposure in PAFR-positive KBP cells, but not in PAFR-negative KBM cells (Figure 4). This direct agonist formation and subsequent PAFR activation also yielded significant ROS generation at 24 hours post-exposure in KBP cells, but not in KBM cells (Figure 6). We also show support for the direct formation of PAF-like lipids in KBP cells from the, sustained, significant ROS generation from 2 to 24 hours post-exposure to Ag-BPEI NPs, whereas KBM cells did not show significant ROS generation after 2 hours (Figure 6).

To confirm the direct formation of PAF-like lipids in PAFR-positive cells, we next utilized HaCaT, human keratinocyte, cells that endogenously express the PAFR. HaCaT cells, like KBP cells, showed significant IL-8 secretion during exposure to 10µg/mL Ag-BPEI NPs at 24-hours (Figure 7), however there was no significant ROS generation seen in HaCaT cells from 2 to 24 hours post-exposure to Ag-BPEI NPs (Figure 8). These results may indicate a cell type-dependent response to PAF-like lipid formation based on variation

in GPC abundance in the plasma membrane or antioxidant enzyme activity between KB (nasopharyngeal) and HaCaT (keratinocyte) cells. There was significant ROS generation at 24 hours post-exposure to 10µg/mL Ag-Citrate NP exposure in HaCaT cells (Figure 8), which was also seen in KBM and KBP cells (Figure 6). This effect is attributed to a higher loss of mitochondrial membrane potential and apoptosis in response to negatively charged NPs being endocytosed and transferred to lysosomes more readily than positively charged NPs (Tomita, 2011). The DCF-DA probe was confirmed as functional from the hydrogen peroxide treatment and the HaCaT cell's PAFR was also shown as functional from its response to 100nM CPAF (Figure 7; Figure 8).

Significant ROS generation was shown during 100nM CPAF exposure in KBP and HaCaT cells 2 hours post-exposure and was followed by a decline of ROS generation (Figure 6; Figure 8). This effect is attributed to homogenous desensitization which inhibits PAFR signaling after abundant receptor activation (Ali, 1999). The elevated ROS generation in KBM cells in response to 100nM CPAF was surprising (Figure 6), however this oxidative stress took place through a PAFR-independent mechanism since there was no significant IL-8 secretion from KBM cells in response to 100nM CPAF exposure and homologous desensitization was not observed (Figure 4a; Figure 6a). Interestingly, we demonstrated an inhibitory effect on CPAF-induced IL-8 secretion by charged Ag NPs. All cell lines were exposed to 100nM CPAF and 10µg/mL Ag-BPEI or Ag-Citrate NPs, at a zero point of addition. At 24 hours post-exposure, we displayed an inhibition of IL-8 secretion in KBP and HaCaT cells during CPAF-induced PAFR activation in the presence

of 10µg/mL Ag-BPEI NPs (Figure 4b; Figure 7). 10µg/mL Ag-Citrate NPs also significantly reduced CPAF-induced IL-8 secretion, but not as much as Ag-BPEI in KBP and HaCaT cells (Figure 5; Figure 7). This anti-inflammatory effect of charged NPs has been reported before in lipopolysaccharide-induced cytokine production in macrophage (raw264.7) cells (Tomita, 2011), however more research needs to be done to understand the mechanism behind this phenomenon.

To further elucidate the inconsistency in ROS generation between KBP and HaCaT cells, we analyzed the uptake dynamics of the cell lines when exposed to Ag-BPEI and Ag-Citrate NPs. We display a PAFR-independent endocytic potential of charged Ag-NPs in epidermal cells (Figure 10). Significant uptake of charged Ag-NPs was shown during the 100 µg/mL exposures in KBM, KBP and HaCaT cells 24 hours post-exposure (Figure 9). Our data supports previously reported ICP-MS results of Ag-NP internalization in fibroblast cells (Wildt, 2016). There was no difference between uptake between any of the cell lines or between NP types within the cell lines, however kinetic differences have been reported in the past between cationic and anionic NPs. Positively-charged NPs have been shown to be endocytosed through non-specific, adsorptive micropinocytosis and to adhere to the negative cell surface of the inner leaflet of the cells plasma membrane (Ono, 1986; Lunov, 2011). This form of endocytosis is clathrin-mediated and once the endosome is internalized, the clathrin coat is lost and recycled into the plasma membrane, while the NPs are within the cell. Kim et al. and Park et al., have shown that polyethyleneimine-functionalized NPs are able to enter the nucleus of the cell and be used to deliver genes as

a non-viral vector (Park, 2010; Kim, 2011) while Ag-BPEI NPs have also been shown to enter the nucleus (Pang, 2015). Depending on the size and surface characteristics of NPs, they will eventually be taken up by lysosomes are dissolved into ions, which causes ROS generation, cytotoxicity and genotoxicity (Asharani, 2009; Cronholm, 2013; Gliga, 2014; Pang, 2015). Furthermore, studies report that negatively-charged NPs are phagocytosed rather than endocytosed due to gram-negative bacteria also holding a negative charge, however they are also endocytosed through clathrin and dynamin-mediated endocytosis (Ono, 1986; Marshal, 1971; Lunov, 2011). The phagocytosed negatively-charged NPs are internalized, delivered to lysosomes and dissolved into ions. The lysosomal dissolution of Ag-NPs in our study does make it difficult to decipher the role of charge in the direct formation of PAF-like lipids from the cytotoxicity that arises from Ag ion leakage inside of the cell. The difference in uptake, distribution and temporal fate may account for the differences we observe in IL-8 secretion and ROS generation between positively and negatively-charged Ag NP exposure.

In the current study, we hypothesize a novel, ROS-independent, pathway of the formation of PAF-like lipids, that act as PAFR agonists, from plasma membrane lipid interactions with amine functionalized Ag-NPs (Figure 1). We postulate that Ag-BPEI NPs interact with the outer and inner leaflet of the plasma membrane, intracellular proteins, organelles and the nucleus once inside of epidermal cells. Once positively-charged NPs cluster at the outer and inner leaflet of the plasma membrane, they cause lipid peroxidation of GPC and form OxGPCs, which activate the PAFR's inflammatory cascade. With more

investigation into direct PAF-like lipid formation from NP exposure, we may harness the ability to form PAFR agonists and remotely induce inflammatory states, which may advance current wound healing therapies.

Endpoint	Cell Line	Ag-BPEI+	Ag-Citrate-
ROS Generation	*KBMock*	↑ (2hr)	↑(8-24hr)
	KBPAFR	↑↑(2-24hr)	↑↑(4-24hr)
	HaCaT	NC	↑(24hr)
IL-8 Secretion/PAFR Activation	*KBMock*	NC	NC
	KBPAFR	↑↑ (5 & 10µg/mL)	NC
	HaCaT	↑(10µg/mL)	NC
Ag-NP Uptake	*KBMock*	≠ HaCaT (100µg/mL)	=
	KBPAFR	=	=
	HaCaT	≠ KBM (100µg/mL)	=

Table 2. Summary of ROS generation, IL-8 secretion and Ag-NP uptake in KBM, KBP and HaCaT cells during exposure to Ag-BPEI and Ag-Citrate NPs.

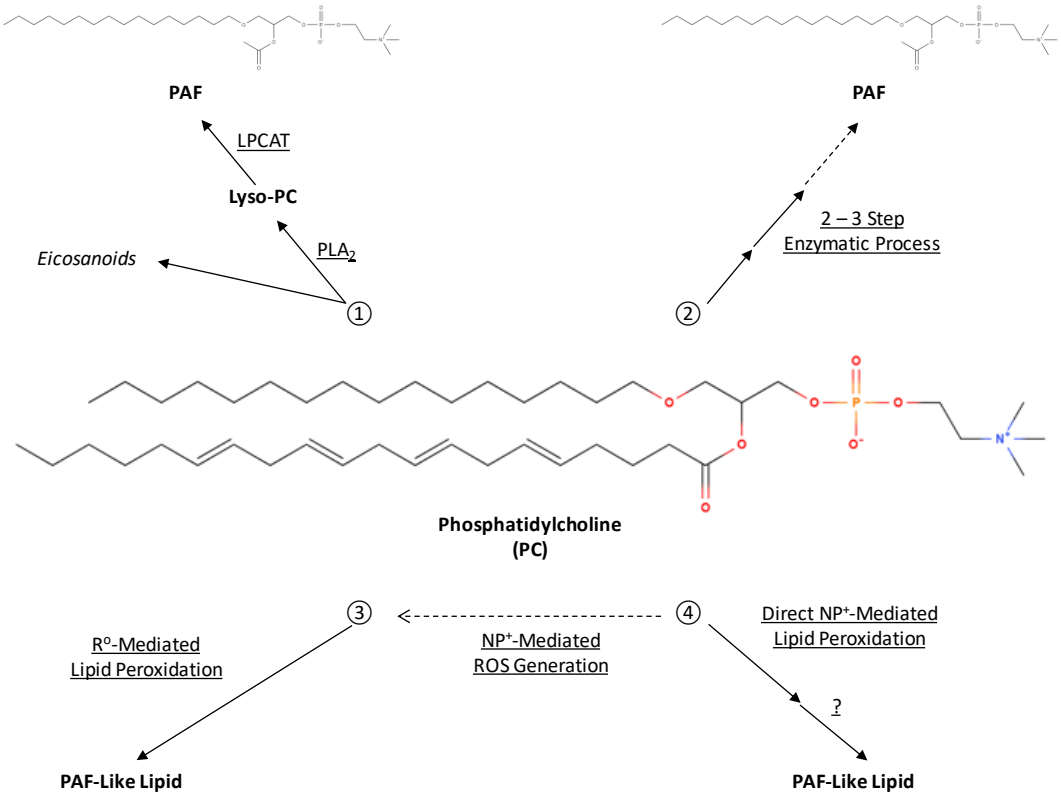

Figure 12. PAF synthesis pathways. Pathway 1 shows the remodeling pathway. Pathway 2 shows the de novo pathway. Pathway 3 shows the lipid peroxidation pathway. Pathway 4 shows our hypothesized NP-mediated pathway of PAF-like lipid synthesis.

Future Direction of the Research

There is much work that can be done to build upon our hypothesis of charge-mediated OxGPC formation. We do not know how the amine groups of the BPEI coating plays a role in lipid peroxidation and how different positively-charged functionalities would affect lipid peroxidation. The future direction of this research is focused on two avenues, which both have to do with further investigating our hypothesized pathway of PAF-like lipid synthesis (Figure 12). The first avenue deals with the positive NPs causing PAF-like lipid formation. We will be conducting the same exposure scenario we show here with cationic and anionic polystyrene NPs, which hold no toxic potential. Eliminating the variable of Ag-ion toxicity will allow us a clearer idea on the ability of NP surface charge to cause PAF-like lipid formation because PAFR activation could also have been due to indirect PAF-like lipid formation. This would begin with ROS-mediated PAF-like lipid formation through lipid peroxidation and subsequent IL-8 secretion. To confirm this, IL-8 secretion would need to be measured 2-hour post-exposure to Ag-NPs to identify whether significant levels were present. Additionally, measuring IL-8 secretion after a NAC and NP co-exposure would give us further support on the role of ROS during our hypothesized synthesis pathway. The second avenue that we will focus on is the measuring of lipid peroxidation with a flurometric assay kit (Abcam; ab118970). This will give us a direct measurement of the extent of lipid peroxidation occurring during NP exposure.

Looking at much earlier timepoints (30 minute) also may be more valuable than looking at a 24-hour exposure, since lipid peroxidation could occur quickly after charged-

NP exposure. Furthermore, utilizing even smaller NPs (5-10nm) would allow for more physiologically practical application to remotely induce inflammation in intact skin.

TEM samples for KBM and KBP cells are on grids and ready to be imaged. The same will be done for HaCaT cells to show internalization and localization at 8 hours post-exposure. Energy-dispersive x-ray spectroscopy will also be performed to confirm that the internalized metals are, in fact, Ag.

Further confocal images of KBM, KBP and HaCaT cells will also be carried out to determine whether there is an increased expression of PAFR in cells exposed to charged Ag-NPs and polystyrene NPs. Image J will be used to count fluorescence of the PAFR and be compared to the control to quantify expression.

Most interestingly, there is also the matter of the anti-inflammatory effect of charged-NPs that we displayed, which has been previously reported (Tomita, 2011). Carrying out 100nM CPAF exposure with 10µg/mL charged Ag-NPs and polystyrene NPs will also be carried out and inflammatory markers will be assessed. If charged NPs are able to cause a PAFR-mediated anti-inflammatory effect, it would support *in vivo* work done in mice that showed improved cognitive ability and reduced neuroinflammation of PAFR-KO mice that received traumatic brain injury (Xiang, 2017).

There is great use for the KB model system in an air-liquid interface (ALI) model as well. Culturing KBM or KBP cells in the apical compartment of the ALI culture and macrophages or neutrophils in the basal compartment of the ALI culture, will allow us to measure the chemotactic potential of NP exposure. We would do this by measuring apical

and basal compartment immune cell concentration in a control well and compare them with an exposed well to measure immune cell recruitment from the basal compartment into the apical compartment. This could serve to advance the KB-PAFR model system by adding an immune component to it. It would also be interesting to determine the effect of substrate stiffness on PAFR activation, PAF-like lipid formation and NP uptake dynamics in KBM, KBP and HaCaT cells.

Works Cited

1. Ai, H., Richardson, R. M., Tomhaves, E. D., Duboses, R. A., Haribabus, B., & Snydermanm, R. (1994). Regulation of Stably Transfected Platelet Activating Factor Receptor in RBL-2H3 Cells. *The Journal of Biological Chemistry*.
2. Ali, H., Richardson, R. M., Haribabu, B., & Snyderman, R. (1999). Chemoattractant receptor cross-desensitization. *Journal of Biological Chemistry*, *274*(10), 6027–6030. https://doi.org/10.1074/jbc.274.10.6027
3. Axelrod, J., Burch, R., & Jelsema, C. (1988). Receptor-mediated activation of phospholipase A 2 via GTP-binding proteins: arachidonic acid and its metabolites as second messengers. *Trends in Neurosciences*, 117–123. Retrieved from http://www.sciencedirect.com/science/article/pii/0166223688901579
4. Barrett, Q. (1984). Calcium Messenger System : An Integrated View, *64*(3).
5. Blank, M. L., Lee, Y. J., Cress, E. A., & Snyder, F. (1988). Stimulation of the de novo pathway for the biosynthesis of platelet-activating factor (PAF) via cytidylyltransferase activation in cells with minimal endogenous PAF production. *Journal of Biological Chemistry*, *263*(12), 5656–5661.
6. Brown, S. L., Jala, V. R., Raghuwanshi, S. K., Nasser, M. W., Haribabu, B., & Richardson, R. M. (2006). Activation and Regulation of Platelet-Activating Factor Receptor: Role of Gi and Gq in Receptor-Mediated Chemotactic,

Cytotoxic, and Cross-Regulatory Signals. *The Journal of Immunology*, *177*(5), 3242–3249. https://doi.org/10.4049/jimmunol.177.5.3242

7. Carlson, C., Hussain, S. M., Schrand, A. M., Braydich-Stolle, L. K., Hess, K. L., Jones, R. L., & Schlager, J. J. (2008). Unique cellular interaction of silver nanoparticles: size dependent generation of reactive oxygen species. *J Phys Chem B*, *112*, 13608–13619. https://doi.org/10.1021/jp712087m
8. Chiltons, F. H., Ellis, J. M., Olson, C., & Wykle, R. L. (1984). 1-O-Alkyl-2-arachidonoyl-sn-glycero-3-phosphochol. *The Journal of Biological Chemistry*, *259*(19), 12014–12019.
9. Cronholm, P., Karlsson, H. L., Hedberg, J., Lowe, T. A., Winnberg, L., Elihn, K., … Möller, L. (2013). Intracellular uptake and toxicity of Ag and CuO nanoparticles: A comparison between nanoparticles and their corresponding metal ions. *Small*, *9*(7), 970–982. https://doi.org/10.1002/smll.201201069
10. Da Silva, I. A., Chammas, R., Lepique, A. P., & Jancar, S. (2017). Platelet-activating factor (PAF) receptor as a promising target for cancer cell repopulation after radiotherapy. *Oncogenesis*, *6*(1), e296-9. https://doi.org/10.1038/oncsis.2016.90
11. Dunn, K., & Edwards-Jones, V. (2004). The role of Acticoat™ with nanocrystalline silver in the management of burns. *Burns*, *30*(SUPPL. 1). https://doi.org/10.1016/S0305-4179(04)90000-9

12. Evers, P. (2018). *Nanotechnology in Medical Applications: The Global Market*. bccResearch. Retrieved from https://www-bccresearch-com.ezproxy.libraries.wright.edu/market-research/healthcare/nanotechnology-medical-applications-market-hlc069d.html
13. Flamand, N., Picard, S., Lemieux, L., Pouliot, M., Bourgoin, S. G., & Borgeat, P. (2006). Effects of pyrrophenone, an inhibitor of group IVA phospholipase A2, on eicosanoid and PAF biosynthesis in human neutrophils. *British Journal of Pharmacology*, *149*(4), 385–392. https://doi.org/10.1038/sj.bjp.0706879
14. Foldbjerg, R., Olesen, P., Hougaard, M., Dang, D. A., Hoffmann, H. J., & Autrup, H. (2009). PVP-coated silver nanoparticles and silver ions induce reactive oxygen species, apoptosis and necrosis in THP-1 monocytes. *Toxicology Letters*, *190*(2), 156–162. https://doi.org/10.1016/j.toxlet.2009.07.009
15. Gliga, A. R., Skoglund, S., Odnevall Wallinder, I., Fadeel, B., & Karlsson, H. L. (2014). Size-dependent cytotoxicity of silver nanoparticles in human lung cells: The role of cellular uptake, agglomeration and Ag release. *Particle and Fibre Toxicology*, *11*(1), 1–17. https://doi.org/10.1186/1743-8977-11-11
16. Han, S. H., Kim, J. H., Seo, H. S., Martin, M. H., Chung, G., Michalek, S. M., & Nahm, M. H. (2006). the Activation of Platelet-Activating Factor Receptor and Jak2. *The Journal of Immunology*, (37). https://doi.org/10.4049/jimmunol.176.1.573

17. Khundkar, R., Malic, C., & Burge, T. (2010). Use of Acticoat™ dressings in burns: What is the evidence? *Burns*, *36*(6), 751–758. https://doi.org/10.1016/j.burns.2009.04.008

18. Kim, E., Lee, J. H., Kim, J. K., Lee, G. H., Ahn, K., Park, J. D., & Yu, I. J. (2015). Case study on risk evaluation of silver nanoparticle exposure from antibacterial sprays containing silver nanoparticles. *Journal of Nanomaterials*, *2015*. https://doi.org/10.1155/2015/346586

19. Kim, J. H., Park, J. S., Yang, H. N., Woo, D. G., Jeon, S. Y., Do, H. J., … Park, K. H. (2011). The use of biodegradable PLGA nanoparticles to mediate SOX9 gene delivery in human mesenchymal stem cells (hMSCs) and induce chondrogenesis. *Biomaterials*, *32*(1), 268–278. https://doi.org/10.1016/j.biomaterials.2010.08.086

20. Li Jeon, N., Baskaran, H., Dertinger, S. K. W., Whitesides, G. M., De Water, L. Van, & Toner, M. (2002). Neutrophil chemotaxis in linear and complex gradients of interleukin-8 formed in a microfabricated device. *Nature Biotechnology*, *20*(8), 826–830. https://doi.org/10.1038/nbt712

21. Marathe, G. K., Davies, S. S., Harrison, K. A., Silva, A. R., Murphy, R. C., Castro-Faria-Neto, H., … McIntyre, T. M. (1999). Inflammatory platelet-activating factor-like phospholipids in oxidized low density lipoproteins are fragmented alkyl phosphatidylcholines. *Journal of Biological Chemistry*, *274*(40), 28395–28404. https://doi.org/10.1074/jbc.274.40.28395

22. MARSHALL, K. C., STOUT, R., & MITCHELL, R. (1971). Mechanism of the Initial Events in the Sorption of Marine Bacteria to Surfaces. *Journal of General Microbiology*, *68*(3), 337–348. https://doi.org/10.1099/00221287-68-3-337
23. Masahiko Hirafuji*, Kazutaka Maeyama**, T. W., & Ogura, and Y. (1988). TRANSIENT INCREASE OF CYTOSOLIC FREE CALCIUM IN CULTURED HUMAN VASCULAR ENDOTHELIAL CELLS BY PLATELET-ACTIVATING FACTOR. *Biochemical and Biophysical Research Communications*, *154*(3), 910–917.
24. Mcintyre, T. M., Reinholdll, S. L., Prescottsq, S. M., & Zimmermans, G. A. (1987). Protein Kinase C Activity Appears To Be Required for the Synthesis of B4 by Human Neutrophi ~ s * Platelet-activating Factor and Leukotriene, 15370–15376.
25. McWilliams, A. (2018). *Nanocomposites, Nanoparticles, Nanoclays and Nanotubes: Global Markets to 2022*. bccResearch. Retrieved from https://www-bccresearch-com.ezproxy.libraries.wright.edu/market-research/nanotechnology/nanocomposites-nanoparticles-nanoclays-and-nanotubes-global-markets-to-2022-nan021h.html
26. Michael J. Holtzman. (1991). Synthesis of the 1-O-hexadecyl molecular species of platelet activating factor by airway epithelial and vascular endothelial cells. *Biochemical and Biophysical Research Communications*, *177*(1).

27. Miura, N., & Shinohara, Y. (2009). Cytotoxic effect and apoptosis induction by silver nanoparticles in HeLa cells. *Biochemical and Biophysical Research Communications*, *390*(3), 733–737. https://doi.org/10.1016/j.bbrc.2009.10.039

28. Pang, C., Brunelli, A., Zhu, C., Hristozov, D., Liu, Y., Semenzin, E., … Zhao, B. (2016). Demonstrating approaches to chemically modify the surface of Ag nanoparticles in order to influence their cytotoxicity and biodistribution after single dose acute intravenous administration. *Nanotoxicology*, *10*(2), 129–139. https://doi.org/10.3109/17435390.2015.1024295

29. Park, J. S., Na, K., Woo, D. G., Yang, H. N., Kim, J. M., Kim, J. H., … Park, K. H. (2010). Non-viral gene delivery of DNA polyplexed with nanoparticles transfected into human mesenchymal stem cells. *Biomaterials*, *31*(1), 124–132. https://doi.org/10.1016/j.biomaterials.2009.09.023

30. Posgai, R., Cipolla-McCulloch, C. B., Murphy, K. R., Hussain, S. M., Rowe, J. J., & Nielsen, M. G. (2011). Differential toxicity of silver and titanium dioxide nanoparticles on Drosophila melanogaster development, reproductive effort, and viability: Size, coatings and antioxidants matter. *Chemosphere*, *85*(1), 34–42. https://doi.org/10.1016/j.chemosphere.2011.06.040

31. Ramesha, C. S., & Pickett, W. C. (1986). Platelet-activating factor and leukotriene biosynthesis is inhibited in polymorphonuclear leukocytes depleted of arachidonic acid. *Journal of Biological Chemistry*, *261*(17), 7592–7595.

32. Ristovski, Z. D., Jayaratne, E. R., Lim, M., Ayoko, G. A., & Morawska, L. (n.d.). INFLUENCE OF THE DIESEL FUEL SULPHUR CONTENT ON THE NANOPARTICLE EMISSIONS FROM A FLEET OF CITY BUSES, (617).
33. Sahu, R. P., Petrache, I., Van Demark, M. J., Rashid, B. M., Ocana, J. A., Tang, Y., … Travers, J. B. (2013). Cigarette smoke exposure inhibits contact hypersensitivity via the generation of platelet-activating factor agonists. *Journal of Immunology (Baltimore, Md. : 1950)*, *190*(5), 2447–2454. https://doi.org/10.4049/jimmunol.1202699
34. Samberg, M. E., Oldenburg, S. J., & Monteiro-Riviere, N. A. (2010). Evaluation of silver nanoparticle toxicity in skin in vivo and keratinocytes in vitro. *Environmental Health Perspectives*, *118*(3), 407–413. https://doi.org/10.1289/ehp.0901398
35. Shen, T. Y., Hwang, S.-B., Doebber, T. W., and Robbins, J. C. (1987). Platelet-activating Factor and Related Lipid Mediators. In *Platelet-activating Factor and Related Lipid Mediators* (pp. 153–190). New York, New York: Plenum Press.
36. Shvedova, A., Castranova, V., Kisin, E., Schwegler-Berry, D., Murray, A., Gandelsman, V., & Baron, P. (2003). Exposure to carbon nanotube material: Assessment of nanotube cytotoxicity using human keratinocyte cells. *Journal of Toxicology and Environmental Health - Part A*, *66*(20), 1909–1926. https://doi.org/10.1080/713853956

37. Tomita, Y., Rikimaru-Kaneko, A., Hashiguchi, K., & Shirotake, S. (2011). Effect of anionic and cationic n-butylcyanoacrylate nanoparticles on NO and cytokine production in Raw264.7 cells. *Immunopharmacology and Immunotoxicology*, *33*(4), 730–737. https://doi.org/10.3109/08923973.2011.565345

38. Travers, J. B. (1999). Oxidative stress can activate the epidermal platelet-activating factor receptor. *Journal of Investigative Dermatology*, *112*(3), 279–283. https://doi.org/10.1046/j.1523-1747.1999.00521.x

39. Whatley, R. E., Nelson, P., Zimmermans, G. A., Stevenst, D. L., Parker, C. J., Mcintyresil, T. M., & Ii, S. M. P. (1989). The Regulation of Platelet-activating Factor Production in Endothelial Cells. *Journal of Biological Chemistry*, *264*(11), 6325–6333.

40. Wildt, B. E., Celedon, A., Maurer, E. I., Casey, B. J., Nagy, A. M., Hussain, S. M., & Goering, P. L. (2016). Intracellular accumulation and dissolution of silver nanoparticles in L-929 fibroblast cells using live cell time-lapse microscopy. *Nanotoxicology*, *10*(6), 710–719. https://doi.org/10.3109/17435390.2015.1113321

41. Yamada, O. (1986). Endocytosis of Cationic and Anionic Iron COlloid Particles by Rat Macrophages, *19*(1), 701-02.

42. Yao, Y., Wolverton, J. E., Zhang, Q., Marathe, G. K., Al-Hassani, M., Konger, R. L., & Travers, J. B. (2009). Ultraviolet B Radiation Generated Platelet-Activating Factor Receptor Agonist Formation Involves EGF-R-Mediated Reactive Oxygen

Species. *The Journal of Immunology*, *182*(5), 2842–2848. https://doi.org/10.4049/jimmunol.0802689

43. Yazdi, A. S., Guarda, G., Riteau, N., Drexler, S. K., Tardivel, A., Couillin, I., & Tschopp, J. (2010). Nanoparticles activate the NLR pyrin domain containing 3 (Nlrp3) inflammasome and cause pulmonary inflammation through release of IL-1 and IL-1 . *Proceedings of the National Academy of Sciences*, *107*(45), 19449–19454. https://doi.org/10.1073/pnas.1008155107
44. Ye, R. D., Prossnitz, E. R., Zou, A., & Cochrane, C. G. (1991). Characterization of a human cDNA that encodes a functional receptor for platelet activating factor. *Biochemical and Biophysical Research Communications*, *180*(1), 105–111. https://doi.org/10.1016/S0006-291X(05)81261-6
45. Yin, X., Chen, Z., Zhu, X., & Hu, J. (2017). Loss of PAFR prevents neuroinflammation and brain dysfunction after traumatic brain injury. *Nature Publishing Group*, (December 2016), 1–12. https://doi.org/10.1038/srep40614
46. Zhang, L. W., Yu, W. W., Colvin, V. L., & Monteiro-Riviere, N. A. (2008). Biological interactions of quantum dot nanoparticles in skin and in human epidermal keratinocytes. *Toxicology and Applied Pharmacology*, *228*(2), 200–211. https://doi.org/10.1016/j.taap.2007.12.022